Supporting Information

A Twist in the Molecular Memory Function: Chemical Compositions of Different Redox Couples Control the Resistive-switching Bias Polarity

Abhik Ghoshal[1], Rajwinder Kaur[1], Sanku Sanju[1], Alok Kumar Singh[2] and Prakash Chandra Mondal[1],*

[1]Department of Chemistry, Indian Institute of Technology Kanpur, Uttar Pradesh-208 016, India

[2]Department of Chemistry, Deen Dayal Upadhyaya Gorakhpur University, Gorakhpur -2730 09, India

E-mail: pcmondal@iitk.ac.in (P.C.M.)

Contents

1. Materials

2,2'-bipyridine and 2,2'-bipyrimidine were purchased from Alfa Aesar and used as received. $RuCl_3.xH_2O$ was purchased from Sigma-Aldrich and stored under a nitrogen atmosphere in a glove box. The precursor complex, *cis*-$[Ru(bpy)_2Cl_2].2H_2O$ was prepared following established procedures. Ferrocene (98%), cobaltocene (98%), anhydrous $FeCl_3$ (98%), and ammonium hexafluorophosphate ($[NH_4][PF_6]$, 99.9%) were purchased from Sigma-Aldrich, India. All glasswares, purchased from Borosil Technology (Mumbai, India), were cleaned with chromic acid and base bath, followed by rinsing with deionized water and drying in an oven at 70°C for 5 hours. The bottom contact in our system is a single-side coated indium tin oxide (ITO) glass substrate from Nano Shel UK Ltd. This substrate is 1.1 mm thick, has a sheet resistance of less than 10 ohms per square, and has over 83% transmittance in the visible range. Throughout the experiment, the ITO substrates were cleaned using anhydrous hexane (99%), acetone (≥ 99%), and isopropyl alcohol (≥99%), all purchased from Finar Limited, India, and purged with nitrogen gas for 20 minutes before electrochemical measurements. Thin films were fabricated using acetonitrile (99%, anhydrous), procured from Rankem, India.

2. Synthesis of Ru-polypyridyl complex

The optical probe was synthesized following a few modifications in the reported synthetic method.[1] An equimolar mixture of $Ru(bpy)_2Cl_2 \cdot 2H_2O$ (55.2 mg, 0.11 mmol) and 2,2'-bipyrimidine (18.03 mg, 0.11 mmol) in absolute ethanol (20 mL) was degassed with N_2 for 15 minutes and then refluxed for 6 hours. After cooling to room temperature, the reaction mixture was filtered. The mixture was then concentrated *in vacuo*, and the residue was dissolved in water. The complex was precipitated by adding a saturated aqueous solution of NH_4PF_6 and collected by vacuum filtration. The resulting powder was dissolved in acetone, filtered, and reprecipitated by the addition of anhydrous ether. After filtration, the complex was purified by column chromatography using alumina (neutral, activity G-III) and acetonitrile-water (90:10, v/v) as the eluent. The second dark orange fraction was collected and dried under vacuum, yielding a dark orange powder. Yield: 57 mg (58%).

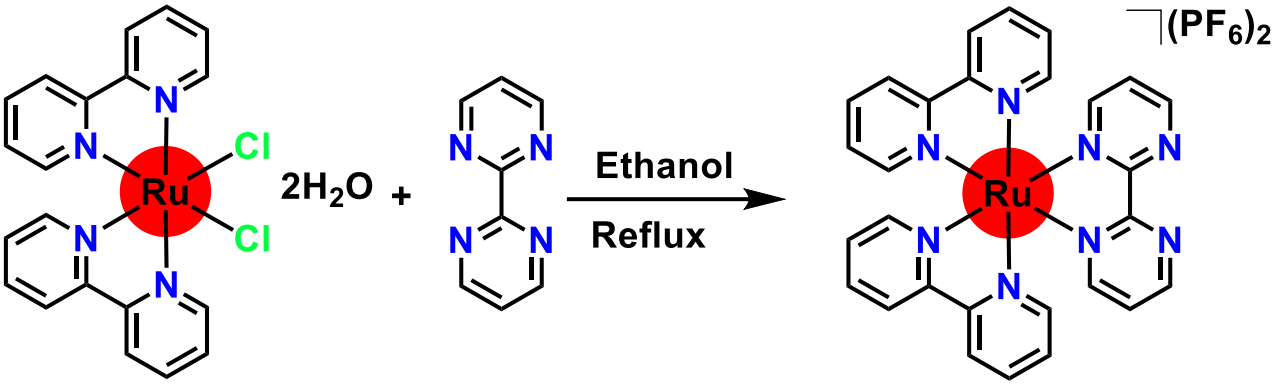

Scheme 1: Synthesis pathway for Ru-polypyridyl complex.

3. Synthesis of ferrocenium hexafluorophosphate

Ferrocene hexafluorophosphate was synthesized according to the literature procedure.[2] To a stirred solution of ferrocene (2.5 g) in a mixture of water (50 mL) and acetone (20 mL) at room temperature was treated with anhydrous $FeCl_3$ (2.95 g). After 15 minutes, the resulting deep blue solution was filtered, and ammonium hexafluorophosphate $[NH_4][PF_6]$ (2.9 g) was added. After an additional 5 minutes, ethanol (25 mL) was added to precipitate the blue solid, which was collected by filtration, yielding 2.8 g of product. This compound is always prepared right before the devices are fabricated.

4. Scan rate-dependent redox parameters of Ru-polypyridyl complex

Table S1. Cathodic and anodic currents ($I_{p,c}$ and $I_{p,a}$), Cathodic and anodic peak potentials ($E_{p,c}$ and $E_{p,a}$), anodic and cathodic current ratio ($\mathbf{I_{p,a}/ I_{p,c}}$), peak to peak separation ($\Delta \mathbf{E_p}$) obtained from the cyclic voltammograms of Ru-polypyridyl complex

S. no.	**Scan rate (mV/s)**	**Anodic peak current ($I_{p,a}$) (mA)**	**Cathodic peak current ($I_{p,c}$) (mA)**	**Anodic peak potential ($E_{p,a}$) (V vs. $Ag/AgNO_3$**	**cathodic peak potential ($E_{p,c}$) (V vs. $Ag/AgNO_3$**	**$I_{p,a}/ I_{p,c}$**	**$\Delta E_p = E_{p,a}- E_{p,c}$ (V) vs. $Ag/AgNO_3$**	**$E_{1/2}= (E_{p,a}+E_{p,c})/2$ (V) vs. $Ag/AgNO_3$**
1.	20	0.123	- 0.122	+ 1.10	+ 1.04	1.01	0.07	+ 1.070
2.	50	0.243	- 0.242	+ 1.10	+ 1.02	1.00	0.06	+ 1.075
3.	100	0.357	- 0.331	+ 1.10	+ 1.02	1.07	0.08	+ 1.060
4.	200	0.489	- 0.481	+ 1.10	+ 1.02	1.01	0.09	+ 1.060

5. Scheme for memory device fabrication

The mixture of Ru-polypyridyl, ferrocene (Fc) and cobaltocene ($Co(Cp)_2$) dissolved in acetonitrile was used for device fabrication. The thin film is fabricated via the drop-casting method. ITO substrates were cleaned via sonication for 15 min in each hexane, acetone, and IPA respectively, purged with nitrogen gas followed by an oxygen plasma cleaning (85 W,10 min.). The molecular thin film was coated on the cleaned ITO substrate and dried in an oven at 40°C for 40 mins. Aluminium as the top contact was deposited using E-beam deposition set-up with a thickness of 100 nm. The current-voltage (I-V) measurements were carried out promptly to ensure accurate results.

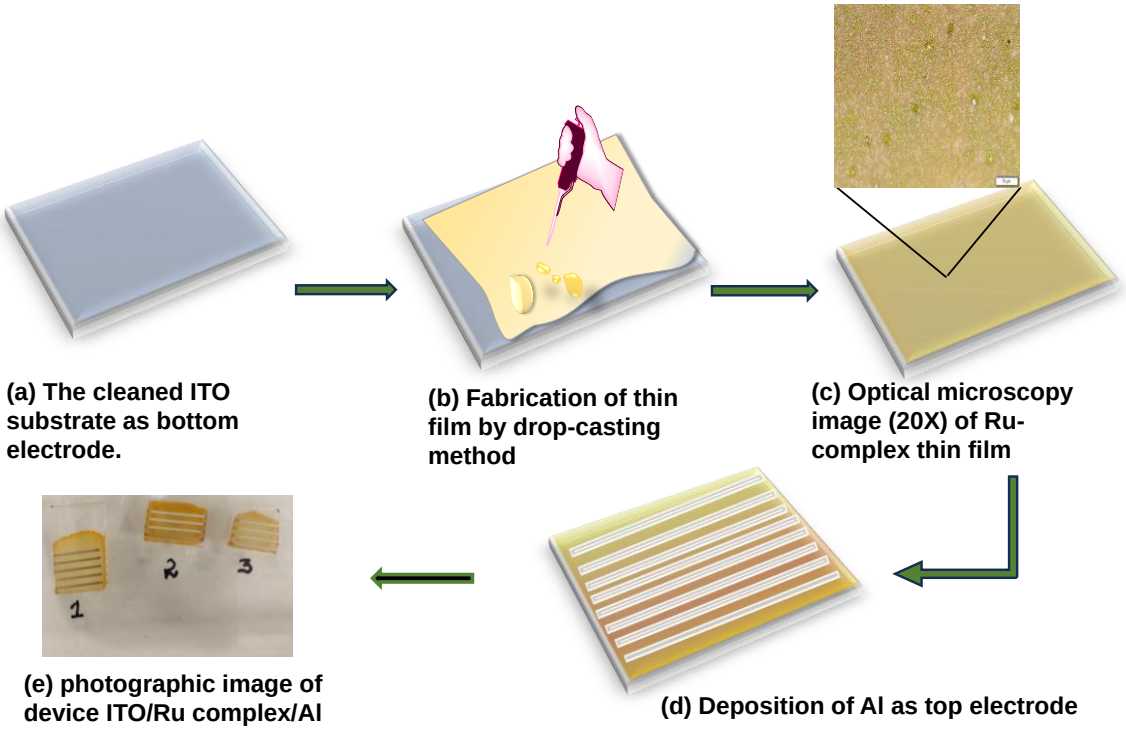

Figure S1. Schematic for fabrication of two-terminal memory device with configuration ITO/active molecular layer/Al. The dimension of ITO was 20 mm x 15 mm, the shadow mask linewidth was 0.5 mm, and gap was 1.5 mm.

6. Optical characterization of Ru-polypyridyl and matrix

The thin film of metal complex shows absorption bands at 424 nm due to the metal-to ligand charge transfer (MLCT) transition. The characteristic absorption signal is highlighted. The UV-Vis spectrum of ferrocenium exhibits a characteristic absorption peak at 616 nm, which gradually diminishes with the addition of cobaltocene. When cobaltocene is added in a 1:1 molar ratio with ferrocenium, peaks at 325 nm and 396 nm, characteristic of cobaltocene, emerge. A new low energy absorption peak at 542 nm arises, which can be a signature of ground-state electronic communication between ferrocenium and cobaltocene moiety. With further increase in cobaltocene concentration, specifically

at a 1:2 molar ratio of ferrocenium to cobaltocene, a distinct low-energy transition appears at 508 nm, corresponding to a d-d transition in cobaltocene. These UV-vis results suggest that cobaltocene chemically reduces the ferrocenium moiety.

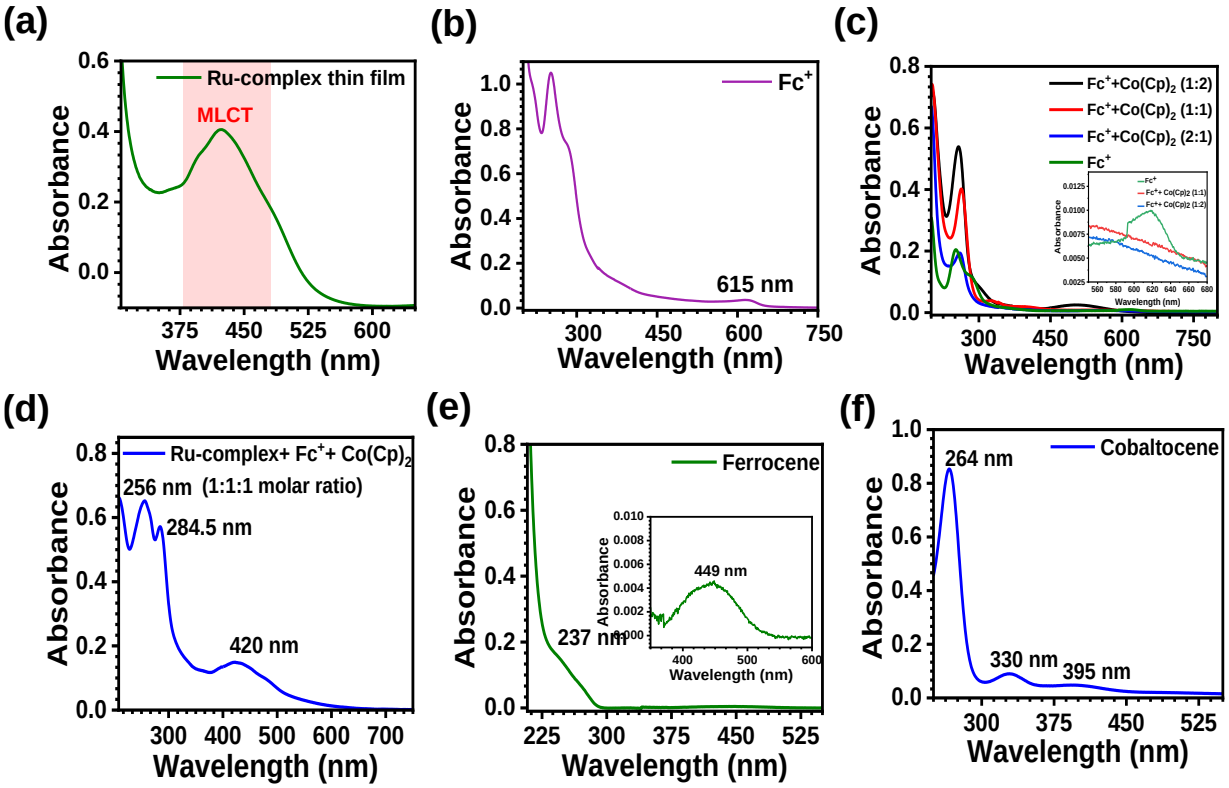

Figure S2. UV-Vis absorption spectrum of (a) ITO/Ru-complex thin film, (b) Fc^+ in acetonitrile solution, (c) Solution phase Fc^+ + $Co(Cp)_2$ at different molar ratio, (d) Ru-complex + Fc^+ + $Co(Cp)_2$ with 1:1:1 molar ratio, (e) ferrocene, and (f) cobaltocene in acetonitrile solution.

Table S2. UV-Vis data for different compositions of Ru-complex, ferrocenium, and cobaltocene recorded in acetonitrile

Compounds	**λ_{max}/nm (ε_{max}/ M^{-1} cm^{-1})**
Ferrocene (Fc)	237 nm (3412), 449 nm (88)
Cobaltocene ($Co(Cp)_2$)	264 nm (17000), 330 nm (1880), 400 nm (940)
Ferrocenium (Fc^+)	251nm (8160 nm), 278 nm (4956), 615 nm (440)
Ferrocenium (Fc^+) + Cobaltocene ($Co(Cp)_2$) (1:1 molar ratio)	263 nm (8000), 325 nm (800), 396 nm (406), 542 nm (168)
Ru-complex +Ferrocenium (Fc^+) + Cobaltocene ($Co(Cp)_2$) (1:1:1 molar ratio)	256 nm (26080), 284.5 nm (22850), 420 nm (6000)

7. Electrochemical characterization of Ru-complex and matrix

Cyclic voltammetry measurements were taken with ITO/Ru-polypyridyl thin film as a working electrode in acetonitrile with scan rates of 20 mV s^{-1}, 50 mV s^{-1}, and 100 mV s^{-1}. For the mixtures, CV was performed in acetonitrile solution. In the case of a 1:1:1 molar mixture of Fc^{+}, $Co(Cp)_2$,and Ru-complex the cathodic peak for ferrocenium was no longer observed. Instead, a redox couple appeared at + 0.11 V and + 0.037 V (vs. $Ag/AgNO_3$), corresponding to the oxidation and reduction of ferrocene, respectively. Additionally, another redox couple at - 1.22 V and - 0.95 V (vs. $Ag/AgNO_3$) was attributed to the redox activity of cobaltocene. The redox peaks associated with ferrocene and cobaltocene in the mixture slightly shift from their pristine values, signifying electronic interactions between different redox moieties.

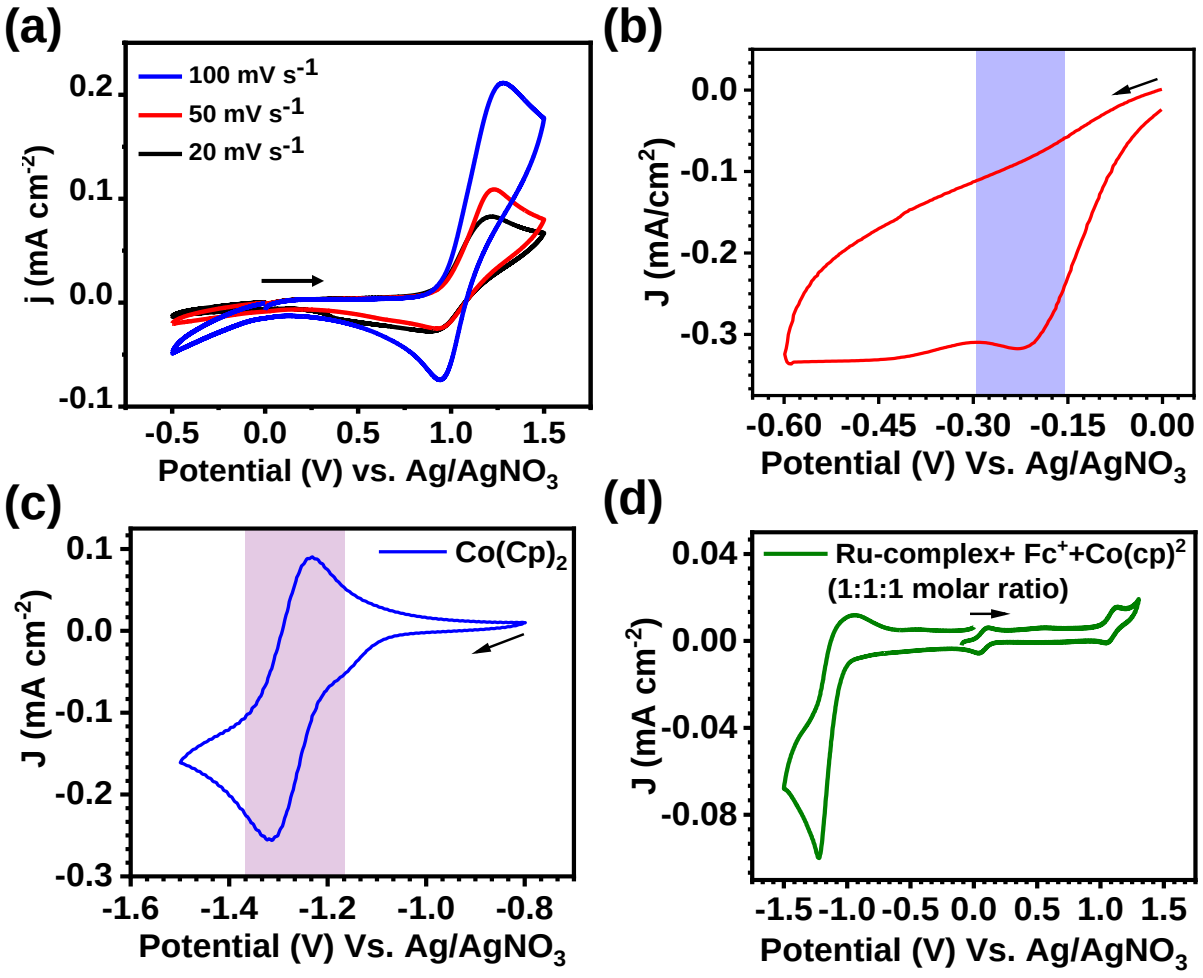

Figure S3. Cyclic voltammogram of (a) Scan rate-dependent CV of Ru-complex thin film deposited on ITO, (b) Fc^{+} in acetonitrile solution, (c) $Co(Cp)_2$, and (d) Ru-complex + Fc^{+} + $Co(Cp)_2$ with 1:1:1 molar ratio in acetonitrile solution using glassy carbon, $Ag/AgNO_3$, and a Pt wire as the working, reference, and counter electrodes, respectively.

Table S3. Redox parameters of different compositions of Ru-complex, ferrocenium and cobaltocene. (All redox potential values are with respect to $Ag/AgNO_3$ reference electrode)

Compounds	E_{ox}/E_{red} (Fe^{II}/Fe^{III})	E_{ox}/E_{red} (Co^{II}/Co^{III})	E_{ox}/E_{red} (Ru^{II}/Ru^{III})
Ferrocene (Fc)	+ 0.075 V/ + 0.001 V	-	-
Cobaltocene ($Co(Cp)_2$)	-	- 1.23 V/ - 1.31 V	-
Fc^+ + $Co(Cp)_2$ (1:1)	+ 0.0965 V/ + 0.018 V	- 1.24 V/ - 1.33 V	-
Fc^+ + $Co(Cp)_2$ + Ru-complex (1:1:1)	+ 0.11 V/ + 0.037 V	- 1.22 V/ - 0.95 V	+ 1.134 V/ + 1.03 V

8. Calculation of HOMO and LUMO for Ru-polypyridyl complex

Energy of Highest occupied molecular orbital (HOMO), lowest unoccupied molecular orbital (LUMO) and band gap were calculated by using the reported procedure.[3] The Tauc plot was made by using UV-Vis data of ITO/ Ru-polypyridyl thin film and was used to calculate optical band gap (2.42 eV). Thin film CV of ITO/ Ru-polypyridyl in the presence of ferrocene was used to calculate the HOMO energy level of the Ru-polypyridyl metal complex. The optical band gap was added to the energy of HOMO to calculate the LUMO energy level of Ru-polypyridyl metal complex.

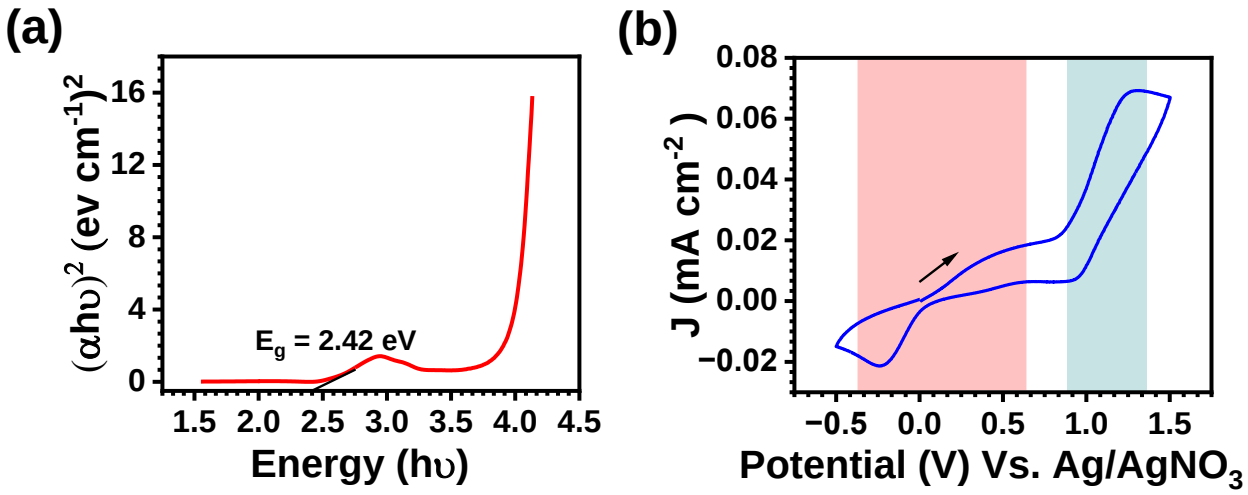

Figure S4. (a) Tauc plot for the Ru-polypyridyl thin film deposited on ITO, and (b) cyclic voltammogram of Ru-polypyridyl thin film in the presence of ferrocene recorded at 100 mV s^{-1} scan rate in 0.1 M of tetrabutylammonium hexafluorophosphate supporting electrolyte in acetonitrile solution using ITO/Ru-polypyridyl, Pt wire and $Ag/AgNO_3$ as working, counter and reference electrodes respectively.

9. X-ray Photoelectron spectra

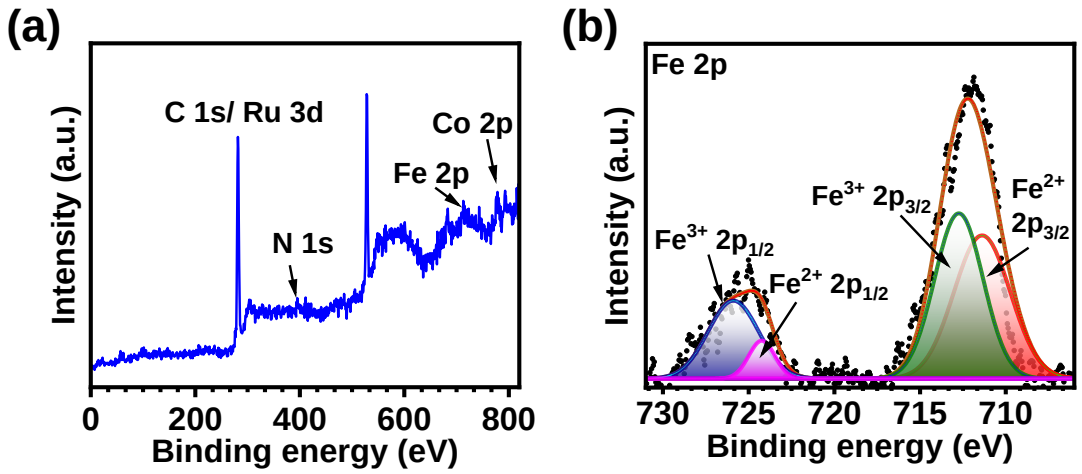

Figure S5. (a) XPS survey scan for ITO/ Ru-complex + Fc + $Co(Cp)_2$, and (b) Fe 2p signal of ITO/Fc^+ + $Co(Cp)_2$ thin film All characteristic signals are highlighted.

Table S4: XPS analysis of ITO/Ru-complex and ITO/Ru-complex + Fc + $Co(Cp)_2$ thin films

S.N.	Material	Element	State/Term	Binding energy (eV)
1.	ITO/Ru-complex	C	1s	284.8± 0.01
				286.1± 0.03
		Ru	$3d_{5/2}$	281.1± 0.02
			$3d_{3/2}$	285.3 ± 0.02
		N	1s	400.3± 1.59
				399.4± 1.32
2.	ITO/Ru-complex + Fc + $Co(Cp)_2$	C	1s	284.80± 0.01
				285.92± 0.01
		Ru	$3d_{5/2}$	281.08± 0.02
			$3d_{3/2}$	285.16± 0.04
		N	1s	400.1± 1.96
				399.4± 1.77
		Fe	$2p_{3/2}$	711.9± 0.01
			$2p_{1/2}$	724.8± 0.01
		Co	$2p_{3/2}$	780.9± 0.02
			$2p_{1/2}$	796.1±0.05

Table S5: Full-width at half-maxima (FWHM) values for XPS signals of ITO/Ru-complex and ITO/Ru-complex + Fc + $Co(Cp)_2$ thin films

Material	Element	State/Term	FWHM (eV)
ITO/Ru-complex	**Ru**	$3d_{5/2}$	1.3± 0.27
		$3d_{3/2}$	1.2± 0.35
ITO/Ru-complex + Fc + $Co(Cp)_2$	**Ru**	$3d_{5/2}$	1.35 ± 0.58
		$3d_{3/2}$	1.35± 0.67
	Fe	$2p_{3/2}$	3.7± 0.13
		$2p_{1/2}$	2.45 ± 0.33
	Co	$2p_{3/2}$	2.1± 0.12
		$2p_{1/2}$	1.84± 0.04

10. Surface morpholy analysis

Field-emission scanning electron microscopy (FE-SEM) analysis shows the compact structure of the molecular layer. The ordering of different redox species present in the film cannot be described based on the FE-SEM data, since the homogeneous mixture of Fc^+, $Co(Cp)_2$ and Ru-complex was drop-casted on ITO substrate.

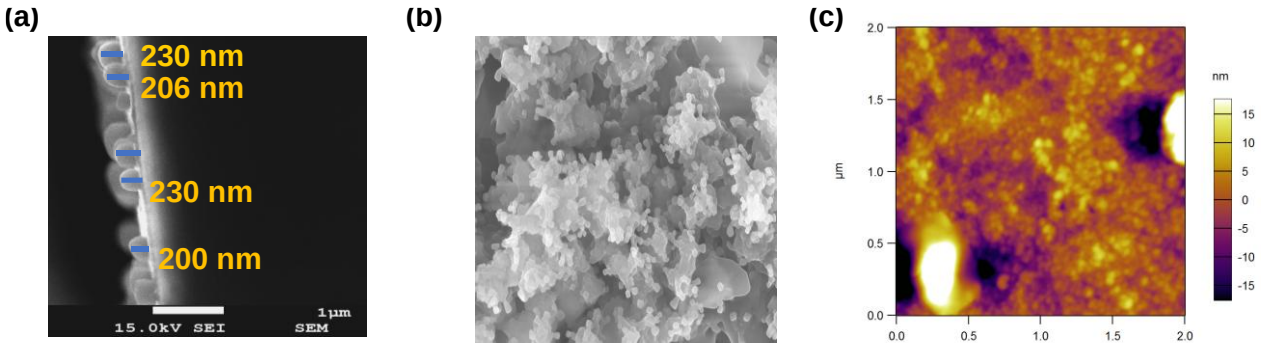

Figure S6. Surface morphological analysis (a) cross-sectional FE-SEM image of ITO/Ru-complex thin film, that was used to calculate the average thickness of the drop-casted molecular thin film. Thickness at five different positions of the layer is highlighted, (b) FE-SEM image with 200 nm scale bar, and (c) 2D AFM image of ITO/Ru-complex + Fc^+ + $Co(Cp)_2$ thin film.

Table S6. Thickness measurement of Ru-polypyridyl thin film

The thickness of the molecular layer of the ITO/Ru-complex thin film was measured at five different positions and the average thickness was calculated.

Thin film	Position 1 (nm)	Position 2 (nm)	Position 3 (nm)	Position 4 (nm)	Position 5 (nm)	Average thickness (nm)
Ru-polypyridyl complex	230	206	216	230	200	216.6± 13.6

11. I-V measurement of the reference device (ITO/Al)

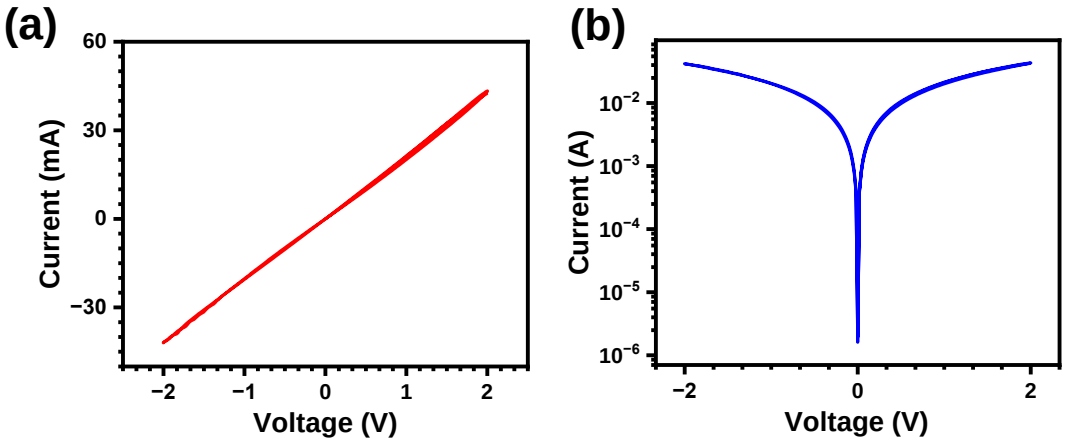

Figure S7. I-V characteristic of device configuration ITO/Al, without any active layer. (a) linear I-V, and (b) log I vs. voltage (V) plots in the bias range ± 2 V.

12. Estimation of switching time of device configuration ITO/Ru-complex/Al

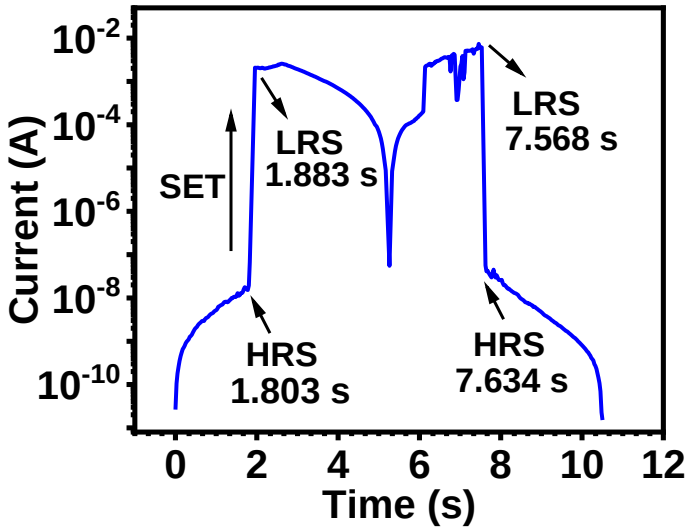

Figure S8. Current (I) vs. time (s) plot of the device configuration ITO/Ru-complex/Al. The switching time associated with the SET and RESET process are mentioned.

13. Cyclic endurance of device configuration ITO/Ru-complex/Al

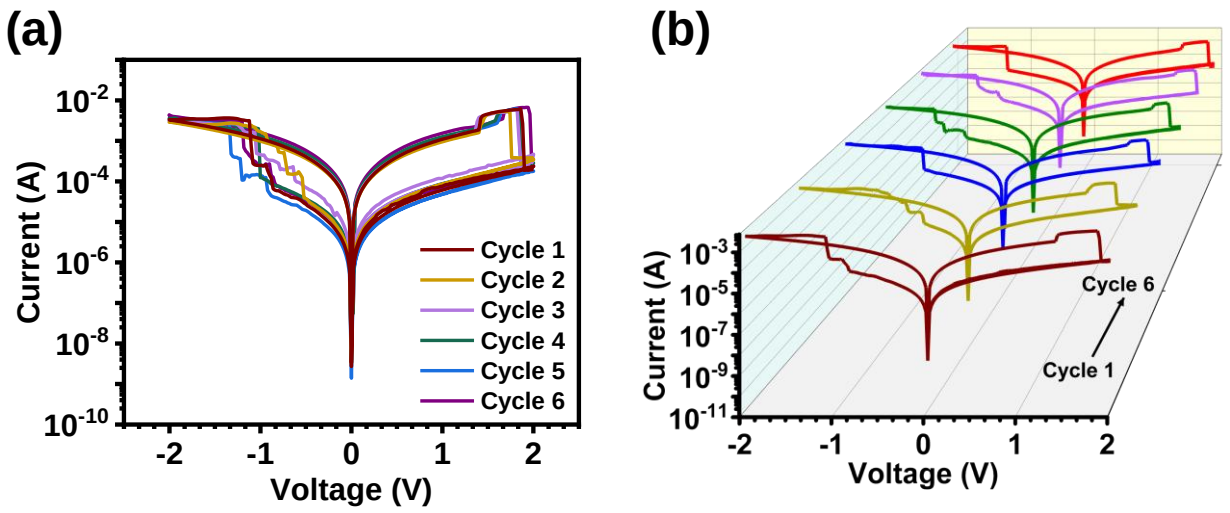

Figure S9. Typical semi-log plot of ITO/Ru-complex/Al device measured up to 6 cycles.

14. Cell-to-cell variation of I-V response for ITO/Ru-complex/Al

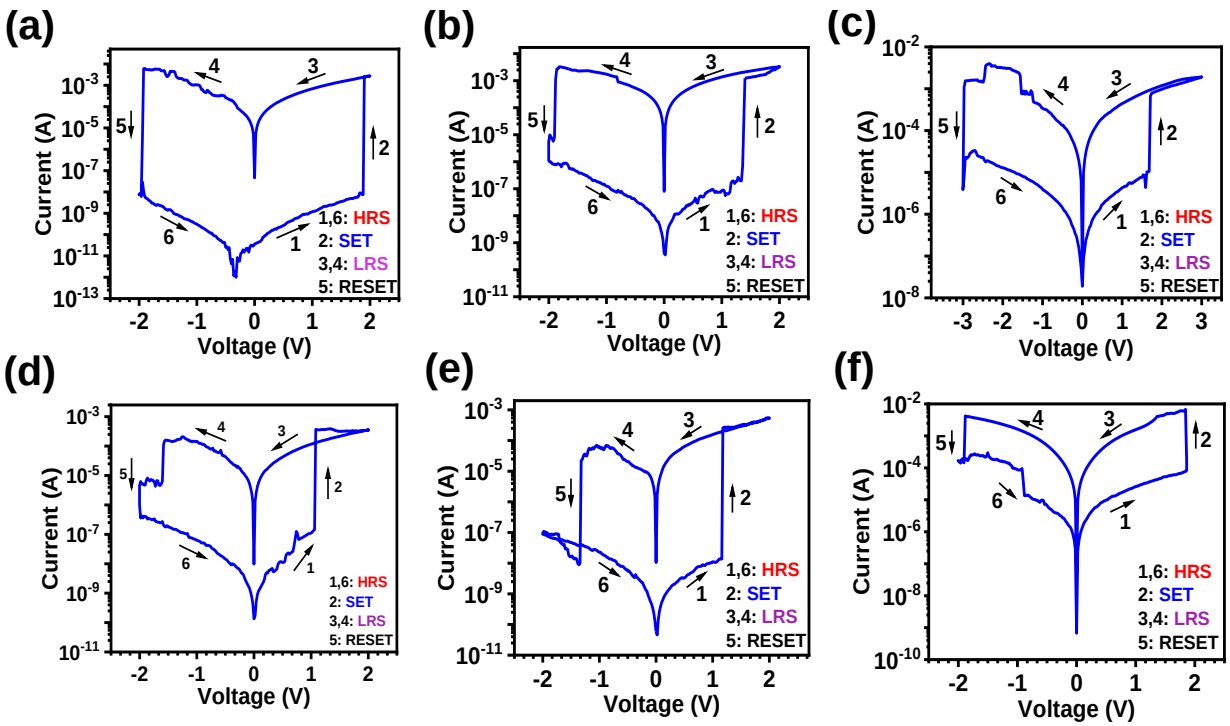

Figure S10. I-V behavior of device configuration ITO/Ru-complex/Al at 6 different junctions (a-f).

15. Endurance and retention study for ITO/Ru-complex/Al

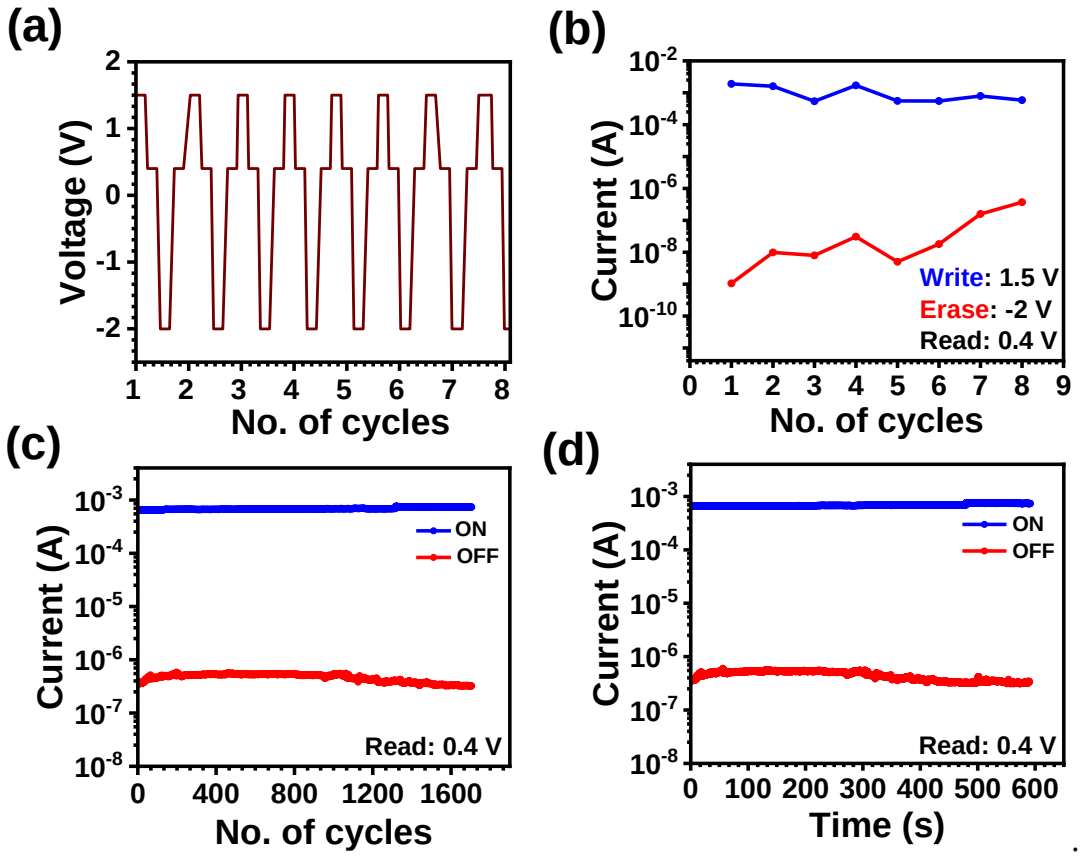

Figure S11. Endurance and retention studies of fabricated ITO/Ru-complex/Al device. (a) Input applied voltage sequence, (b) output current responses during repeated **W**rite/**R**ead/**E**rase/**R**ead (+ 1.5 V/ + 0.4 V/ - 2.0 V/ + 0.4 V) cycles. (c) retention study of the device in 'OFF' and 'ON' states over 17× 10^2 cycles, and (d) The stability of 'OFF' and 'ON' currents for 600 s.

16. I-V characteristic for ITO/Ru-complex + Fc + Co $(Cp)_2$/Al

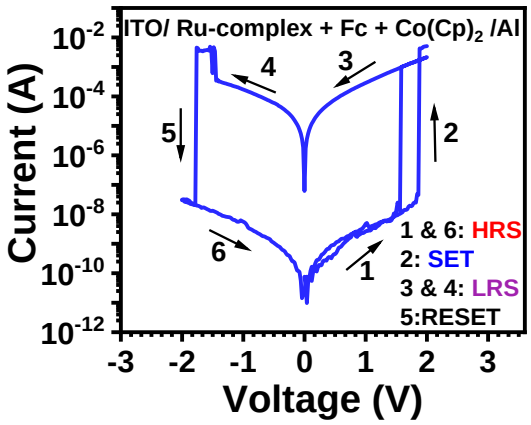

Figure S12. Semi-log I-V plot of device configuration ITO/Ru-complex + Fc + $Co(Cp)_2$/Al (molar ratio 1:1:1 of individual components) in the bias range ± 2 V.

17. $I_{ON/OFF}$ ratio vs. voltage of the system

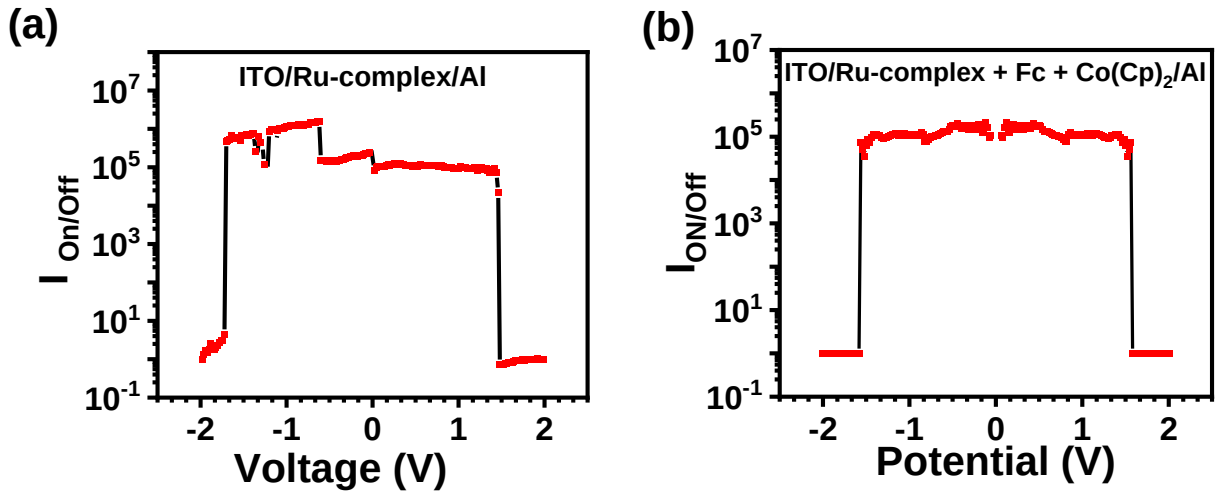

Figure S13. $I_{ON/OFF}$ ratio vs. voltage of the memory device configuration of (a) ITO/Ru-complex/Al, and (b) ITO/Ru-complex + Fc + $Co(Cp)_2$/Al.

18. I-V characteristic of the fabricated RRAM devices for the control experiment

18.1. I-V characteristic of device configuration ITO/Ru-complex + Fc/Al

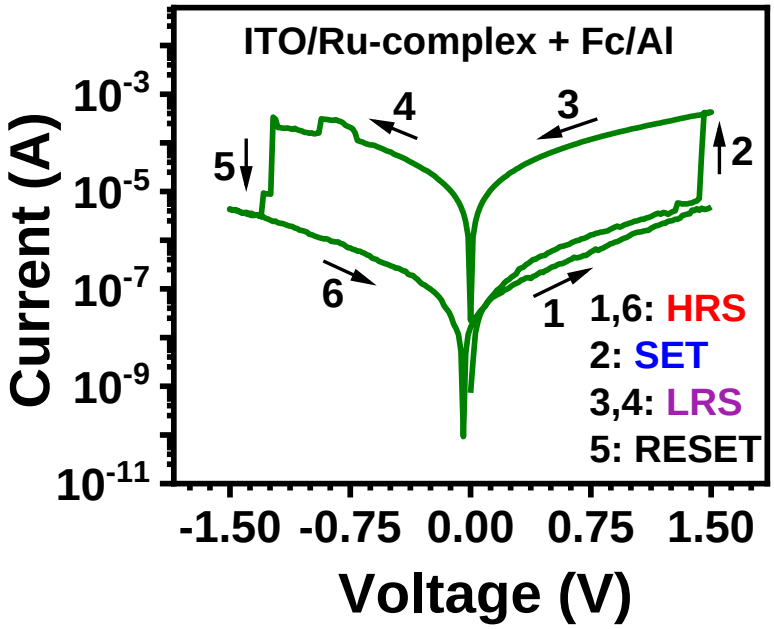

Figure S14. Semi-log I-V plot of device configuration ITO/Ru-complex + Fc/Al in the bias range ± 1.5 V.

18.2. I-V characteristic of device configuration ITO/Ru-complex + $Co(Cp)_2$/Al

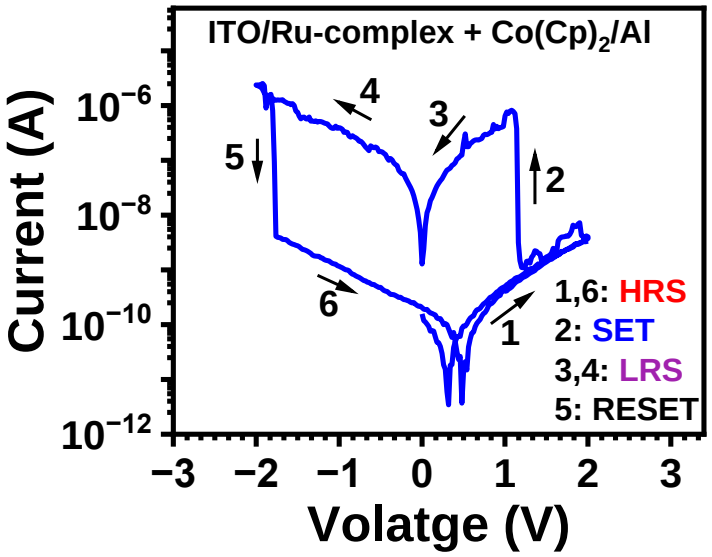

Figure S15. Semi-log I-V plot of device configuration ITO/Ru-complex + $Co(Cp)_2$/Al in the bias range $\pm$ 2 V.

19. Cyclic endurance for ITO/Ru-complex + Fc^+ + $Co(Cp)_2$/Al at 1:1:1 molar ratio

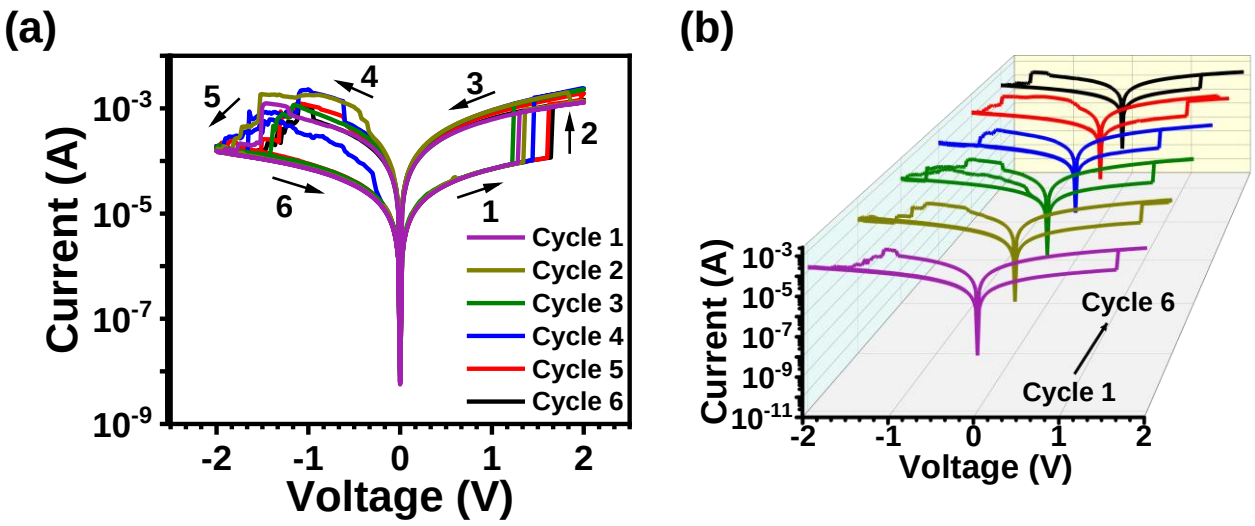

Figure S16. Typical semi-log plot of ITO/ Ru-complex + Fc^+ + $Co(Cp)_2$/ Al device measured up to 6 cycles.

20. Endurance and retention study for ITO/Ru-complex+ Fc^+ + $Co(CP)_2$/Al with 1:2:2 molar ratio

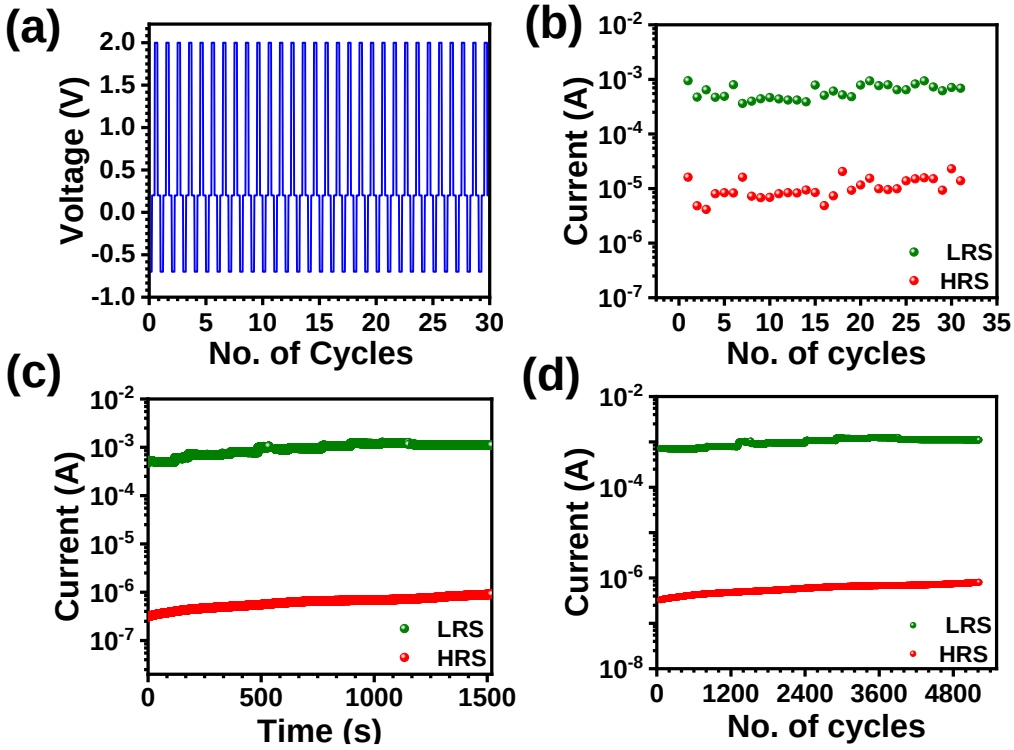

Figure S17. Endurance and retention studies of fabricated **ITO/Ru-complex+ Fc^+ + $Co(CP)_2$/Al** device. (a) Input applied voltage sequence, (b) output current responses during repeated **W**rite/**R**ead/**E**rase/**R**ead (- 0.7 V/+ 0.2 V/+ 2.0 V/+ 0.2 V) cycles. (c) The stability of 'OFF' and 'ON' currents for 1500 s, and (d) retention study of the device in 'OFF' and 'ON' states over 5×10^3 cycles.

21. I-V measurements for ITO/Fc^+ + $Co(Cp)_2$/Al and ITO/ Fc^+/Al

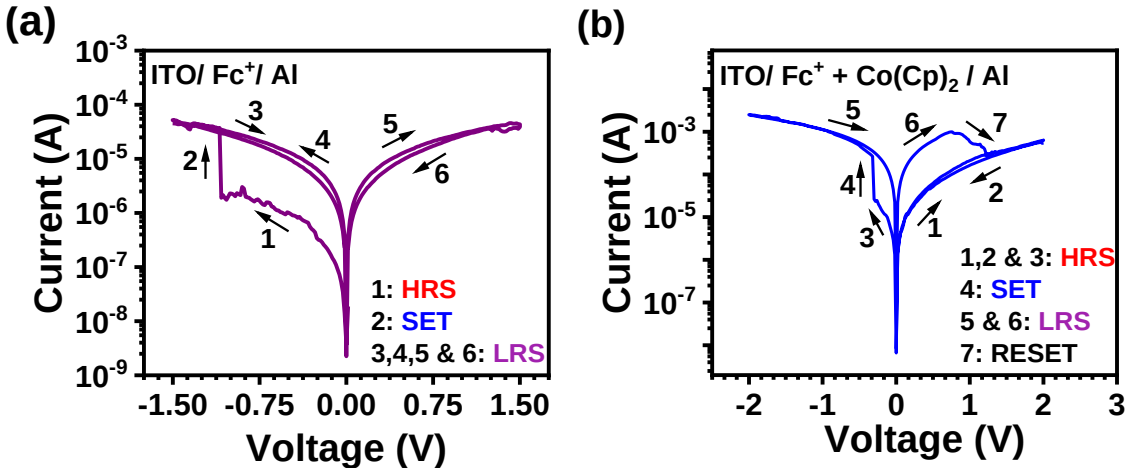

Figure S18. Semi-log I-V plot of device configuration (a) ITO/Fc^+/Al, and (b) ITO/Fc^+ + $Co(Cp)_2$/Al in the bias range $\pm$ 1.5 V and $\pm$ 2V respectively.

22. Demonstration of Pavlov's learning experiment

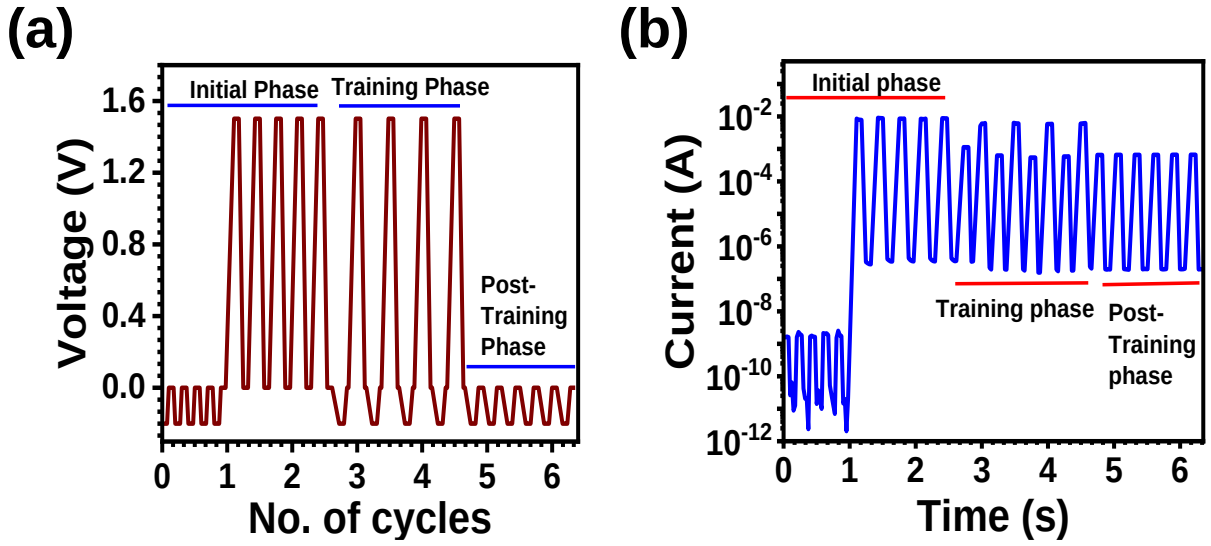

Figure S19. Demonstration of associative learning experiment. (a) Voltage pulse sequence, (b) current response for the initial phase, training period, and post-training phase.

23. Statistical data of memory devices: performance and yield

Table S7. Comparative performance of RRAM devices of different configuration

S.No.	Type of device	V_{SET} (V)	V_{RESET} (V)	Power consumption	
				SET	RESET
1.	ITO/Ru-complex/Al	+ 1.4	- 1.7	26.6 nW	10.2 mW
2.	ITO/Ru-complex + Fc + $Co(Cp)_2$/Al (1:1:1)	+ 1.5	- 1.7	19.3 nW	7.4 mW
3.	ITO/Ru-complex + Fc^+ + $Co(Cp)_2$/Al (1:1:1)	+ 1.7	- 1.6	0.6 µW	11.2 mW
4.	ITO/Ru-complex + Fc^+ + $Co(Cp)_2$/Al (1:2:2)	- 0.3	+ 1.6	6.6 µW	32 mW
5.	ITO/ Fc^+ + $Co(Cp)_2$/Al	- 0.3	+ 0.75	7.9 µW	0.75 mW
6.	ITO/ Fc^+/Al	- 1.08	-	2.05 µW	-

Table S8: Statistical data of RRAM devices of different configuration

Type of device	No. of devices fabricated	No. of devices worked	Yield (%)	Threshold voltage (V)		ON/OFF ratio
				SET	RESET	
ITO/Ru-complex/Al	15	10	66.7	+ 1.65± 0.4	- 1.72± 0.6	10^4
ITO/Ru-complex + Fc + $Co(Cp)_2$/Al (1:1:1)	12	8	66.6	+ 1.71± 0.3	- 1.90± 0.7	10^4
ITO/Ru-complex + Fc^+ + $Co(Cp)_2$/Al (1:1:1)	14	9	64.3	+ 1.48± 0.6	- 1.55± 0.8	10^3
ITO/Ru-complex + Fc^+ + $Co(Cp)_2$/Al (1:2:2)	10	7	70.0	- 0.50± 0.3	+ 1.65± 0.4	10^2

Table S9: **Comparison table of metal-polypyridyl based RRAM device performance**

S. No.	Device configuration	Switching threshold (V)		ON/OFF ratio	References
		SET	RESET		
1.	ITO/Ru-complex/Al	+ 1.4	- 1.7	10^5	This work
2.	Al/$[(Phen)_2Cr(Me_4Phen)](OTf)_3$/Al	+ 4.6	- 4.8	10^4	Kandasamy et al.[4]
3.	Al/$[Cr(bpy)_2(Br_2bpy)](OTf)_3$/Al	+ 1.2	-	150	Kandasamy et al.[4]
4.	Al/$[Cr(bpy)_2(COOMebpy)](OTf)_3$/Al	+ 2.6	-	20	Kandasamy et al.[4]
5.	Al/Ru^{2+}-complex/ITO	+ 4	-	10^4	Leung et al.[5]
6.	ITO/$Ru^{II}(bpy)_2(L)_2$/Al	- 1.3	+ 1.0	10^3	Pradhan et al.[6]
7.	$[Ru((phenylazo)pyridine)_3](PF_6)_2$	+ 4	- 4	10^4	Goswami et al.[7]
8	ITO/ $[(tpy)Ru(tppz)Ru(tpy)](PF_6)_4$/Al	+ 3.4	- 4.3	10^2-10^3	Cui et al.[8]
9	Ta/$EV(ClO_4)_2$ + PEO/TPy-Fe/ITO	+ 3.0	- 2.0	10	Yang et al.[9]

10	ITO/Au Np/[Ru((phenylazo)pyridine)$_3$](PF$_6$)$_2$/ITO	+ 0.52	- 0.55	10^5	Goswami et al.[7]
11	ITO/Fc-2,7-diethynylfluorene derivative/Al	- 1	+ 2	10^4	Xiang et al.[10]
12	Al/[(Phen)$_2$Cr (Me$_2$bpy)](OTf)$_3$/Al	+ 2.8	- 2.2	10^6	Kandasamy et al.[4]
13	ITO/Au[Ru((phenylazo)pyridine)$_3$](PF$_6$)$_2$/C-AFM	+ 0.1	$\sim -$ 0.3	10^3	Goswami et al.[7]
14	Ag/keratin/FTO	+ 1.5V	- 1V	10^3	Lin et al.[11]
15	Al/GO-PVK/ITO	- 2V	+ 3.5V	10^2	Liu et al.[12]
16	Au/aniso-TPDAP/Au/SiO2/Si	+ 3V	- 1.5V	$\sim 10^4$	Kim et. al[13]
17	Al/(bis-4-(N-carbazolyl)phenyl)phenylphosphine oxide/ITO	+ 3.2V	- 3.8V	10^4	Mao et al.[14]
18	Ag/PMMA/BiI$_3$/PMMA/Au	Forming - 0.66V, SET: 0.26 V	- 0.23 V	$\sim 10^8$	Chen et al.[15]

24. EIS derived electrical parameters

Table S10: Value of Fitting parameters obtained from EIS data using Randles equivalent circuit

Element	ITO/Ru-complex/Al	ITO/ Ru-complex + Fc + Co(Cp)$_2$/Al
R_u (Ω)	94,680	92800
Rct (Ω)	1.529×10^7	1.633×10^7
Y_0 -1 (S*s^a)	8.43×10^{-9}	8.43×10^{-9}
a-1	902.59×10^{-3}	900.82×10^{-3}

25. References:

1 A. Kumar, M. Chhatwal, A. K. Singh, V. Singh and M. Trivedi, *Chem. Commun.*, 2014, **50**, 8488–8490.

2 M. Deb, S. Hazra, P. Dolui and A. J. Elias, *ACS Sustain. Chem. Eng.*, 2019, **7**, 479–486.

3 A. Shafiee, M. M. Salleh and M. Yahaya, *Sains Malaysiana*, 2011, **40**, 173–176.

4 B. Kandasamy, G. Ramar, L. Zhou, S. T. Han, S. Venkatesh, S. C. Cheng, Z. Xu, C. C. Ko and V. A. L. Roy, *J. Mater. Chem. C*, 2018, **6**, 1445–1450.

5 M. Y. Leung, S. Y. L. Leung, D. Wu, T. Yu and V. W. W. Yam, *Chem. - A Eur. J.*, 2016, **22**, 14013–14021.

6 B. Pradhan and S. Das, *Chem. Mater.*, 2008, **20**, 1209–1211.

7 S. Goswami, A. J. Matula, S. P. Rath, S. Hedström, S. Saha, M. Annamalai, D. Sengupta, A. Patra, S. Ghosh, H. Jani, S. Sarkar, M. R. Motapothula, C. A. Nijhuis, J. Martin, S. Goswami, V. S. Batista and T. Venkatesan, *Nat. Mater.*, 2017, **16**, 1216–1224.

8 B. Bin Cui, Z. Mao, Y. Chen, Y. W. Zhong, G. Yu, C. Zhan and J. Yao, *Chem. Sci.*, 2015, **6**, 1308–1315.

9 X. Yang, C. Wang, J. Shang, C. Zhang, H. Tan, X. Yi, L. Pan, W. Zhang, F. Fan, Y. Liu, Y. Chen, G. Liu and R. W. Li, *RSC Adv.*, 2016, **6**, 25179–25184.

10 J. Xiang, T. K. Wang, Q. Zhao, W. Huang, C. L. Ho and W. Y. Wong, *J. Mater. Chem. C*, 2016, **4**, 921–928.

11 Q. Lin, S. Hao, W. Hu, M. Wang, Z. Zang, L. Zhu, J. Du and X. Tang, *J. Mater. Chem. C*, 2019, **7**, 3315–3321.

12 G. Liu, X. Zhuang, Y. Chen, B. Zhang, J. Zhu, C. X. Zhu, K. G. Neoh and E. T. Kang, *Appl. Phys. Lett.*, 2009, **95**, 253301.

13 J. Kim, H. Ohtsu, T. Den, K. Deekamwong, I. Muneta and M. Kawano, *Chem. Sci.*, 2019, **10**, 10888–10893.

14 J. Y. Mao, L. Zhou, Y. Ren, J. Q. Yang, C. L. Chang, H. C. Lin, H. H. Chou, S. R. Zhang, Y. Zhou and S. T. Han, *J. Mater. Chem. C*, 2019, **7**, 1491–1501.

15 M. H. Chen, P. F. Lin, B. Y. Chen and J. F. Cheng, *ACS Appl. Electron. Mater.*, 2023, **5**, 255–264.